

Absorption features in the quasar HS 1603+3820 II. Distance to the absorber from photoionisation modelling

A. Róžańska^{a,*}, M. Nikołajuk^b, B. Czerny^a, A. Dobrzycki^c, K. Hryniewicz^a, J. Bechtold^d, H. Ebeling^e

^a*N. Copernicus Astronomical Center, Bartycka 18, 00-716 Warsaw, Poland*

^b*Faculty of Physics, University of Białystok, Lipowa 41, 15-424 Białystok, Poland*

^c*European Southern Observatory, Karl-Schwarzschild-Strasse 2, D-85748 Garching bei München, Germany*

^d*Steward Observatory, University of Arizona, Tucson, AZ 85721, USA*

^e*Institute for Astronomy, University of Hawai'i, 2680 Woodlawn Drive, Honolulu, HI 96822, USA*

Abstract

We present photoionisation modelling of the intrinsic absorber in the bright quasar HS 1603+3820. We construct broad-band spectral energy distribution using optical/UV/X-ray observations from different instruments as an input to photoionisation calculations. Spectra from Keck telescope show extremely high ratio of C IV to H I for the first absorber in system A, named A1. This value, together with high column density of C IV ion, puts strong constraints on photoionisation model. We use two photoionisation codes to derive hydrogen number density at the cloud illuminated surface. Estimating bolometric luminosity of HS 1603+3820, from typical formula for quasars, we calculate the distance to A1. Either for constant density cloud (modelled by CLOUDY), or stratified cloud (modelled by TITAN) we were able to find a single photoionisation solution, assuming solar abundances, which explains both the ionic column density of C IV, and high C IV to H I ratio. The derived location is as close as 0.1 pc, and situates an absorber even closer to the nucleus than the possible location of the Broad Line Region in this object. The upper limit for the distance is sensitive to the adopted covering factor and the carbon abundance. Photoionisation modelling always prefers dense clouds with the number density $n_0 = 10^{10}, 10^{12} \text{ cm}^{-3}$, to explain observational constraints of HS 1603+3820 intrinsic absorption. This number density is of the same order as the number density in the disk atmosphere at the implied distance of the A1. Our results thus show that the disk wind escaping from outermost accretion disk atmosphere can build up dense absorber in quasars.

Keywords: (galaxies:) quasars: absorption lines, atomic processes, radiative transfer, (galaxies:) quasars: individual (HS 1603+3820)

1. Introduction

High resolution optical/UV spectra show that over 20% of quasars exhibit broad absorption lines (BALs) from ionised species of heavy elements. In some objects lines are from high-ionisation species, as C IV, N V, O VI forming subclass of HiBALs, and in other cases absorption features originate from low-ionisation species as Mg II, Al II, Si II, Fe II forming LoBALs subclass.

In all BALs, lines can exhibit very complex blueshifted profiles, indicating the presence of several absorbing systems moving toward an observer with different velocities, for example in QSO 2359-1241 (Arav et al., 2001). Narrow line components indicate usually velocities of the order of a few hundred km s^{-1} , while velocities of some broad lines can reach even $50,000 \text{ km s}^{-1}$ (Weymann, 1995).

Similar absorption in UV is observed in Seyfert galaxies (Crenshaw et al., 1999). Moreover, in 50% of those objects, the matter at higher ionisation state, so called “warm absorber”, is detected in X-ray band, for example in NGC 3783 (Kaspi et al., 2001). Observed spectral features from O VIII, Mg XII, Si XIV, and even Fe XXV indicate

*Principal corresponding author

Email address: agata@camk.edu.pl (A. Róžańska)

temperature of an absorbing gas to be of the order of $10^6 - 10^7$ K. Typical “warm” X-ray lines are narrower than those of BALs, and blueshifted by velocities of the order of few hundreds km s^{-1} up to 10^3 km s^{-1} (for review, see Blustin et al., 2005).

Many questions arise about the origin and physical conditions of those outflows. The first obvious is: does the UV and X-ray absorption occur in the same wind? There are two examples showing that the line detected in X-rays can be fitted exactly by the same velocity profile as the line detected in UV for two active galaxies NGC 5548 and NGC 3783 (Kaastra et al., 2002; Gabel et al., 2003). In general, to answer this question we have to collect multiband optical/UV/X-rays observations of quasars with resolution high enough to compare line profiles from different energy bands. However, presently working satellites as *Chandra* and *XMM-Newton* are not able to detect X-ray absorption in distant quasars, and very often X-ray spectrum can be modelled only as a power-law, like in case of *Chandra* detection of HS 1603+3820 (Dobrzycki et al., 2007, hereafter Paper I).

Physical conditions in UV or X-ray absorbing clouds can be studied by photoionisation modelling. For that purpose, a broad-band spectral energy distribution (SED) of a considered source is needed. Nevertheless, many observations do not cover EUV band. For this reason in several recent papers on UV outflows, authors have used standard Mathews and Ferland (1987) composite quasar spectrum for photoionisation modelling. It is widely known, that the SED of incident photons determines ionisation and thermal structure of the absorbing plasma (Róźańska et al., 2008; Chakravorty et al., 2009). In this paper, taking into account multi-wavelength observations of HS 1603+3820 from *MMT*, *Keck* and *Chandra* telescopes we have constructed the SED of the quasar spectrum. This SED is used as an input for our advanced photoionisation modelling of the system using codes *CLOUDY* and *TITAN*.

Photoionisation modelling provides us with a possibility to determine the distance of the cloud from the nucleus, only if the SED is dominated by soft disk component, as shown in Róźańska et al. (2008). Photoionised models depend predominantly on the ionisation parameter, i.e. a combination of the surface number density and a distance from the source. Models illuminated by only hard X-ray power-law are degenerated for the gas number density up to 10^{11} cm^{-3} . In this case, we are not able to differentiate between matter located closer to the nucleus with higher density, and more diluted gas being farther away. The transmitted spectra through such two clouds look the same, since their ionisation and temperature structure are identical (Róźańska et al., 2008). In case of HS 1603+3820, where the SED is dominated by soft UV emission over X-rays, this degeneracy is broken due to the fact that the Comptonization becomes not important comparing to the free-free processes (Róźańska et al., 2008). Therefore, the hydrogen number density at the cloud surface can be estimated from the line ratios, and this density together with quasar luminosity, and ionisation parameter gives us a distance of an absorber from the source of continuum.

Our method is complementary to other two methods used for distance derivation, based on different ways of determining the density number at an absorbing cloud surface. In the first one, it can be done from variability data, assuming that observed spectral changes are due to variation of the ionisation state (Krolik and Kriss, 1995). This method allowed us to estimate the number density of the warm absorber in Seyfert 1 galaxy NGC 4055 from ROSAT data to be of the order of $n = 10^8 \text{ cm}^{-3}$, implying the location of the gas at about $R = 0.0024 \text{ pc}$ (Nicastro et al., 1999). Nevertheless, in case of NGC 3783 two groups using this method got opposite results. Netzer et al. (2003) have found clouds at three different ionisation levels located on 3.2, 0.63, and 0.18 pc from the nucleus, while Krongold et al. (2005) found two clouds on 0.0029, and 0.0004-0.0008 pc, using the same 900 ks *Chandra* observations. Outflowing velocities of that absorbers were of the order of 750 km s^{-1} .

The second method uses high quality UV spectra of LoBALs, since number density can be estimated by comparing the ionic column densities of excited metastable states to their ground states of the most popular ions He I, C II, Si III, and Fe II (Korista et al., 2008; Moe et al., 2009; Bautista et al., 2010). In case of three quasars presented in above papers, estimated number density is always of the order of $10^3 - 10^{4.4} \text{ cm}^{-3}$, indicating the gas location at about 3-6 kpc. The velocities of those absorbers are in the range of $1400-7500 \text{ km s}^{-1}$.

In this paper we perform photoionisation modelling of an intrinsic absorption in quasar HS 1603+3820 with the aim to determine physical properties of an absorbing gas. This HiBAL type object is interesting since the ratio of C IV to H I was found to be extremely high - above 20 (Paper I). The most interesting absorbing systems are outflowing with velocities reaching 3000 km s^{-1} . By comparison of model parameters to those indicated from observations of HS 1603+3820, we are able to find a single photoionisation solution, which can explain observed ionic column densities of the first cloud in system A, reported in Paper I and marked as A1 here.

We use photoionisation modelling to determine uniquely both the hydrogen number density at the illuminated surface of the cloud, and the ionisation parameter. Those two quantities combined with the source luminosity allow us

to compute the distance from the central nucleus to the absorbing system. We present such calculations in this paper and compare results with previous estimations done by Misawa et al. (2005, 2007).

This paper is organised as follows: in Sec. 2 we present the source, and in Sec. 3 we review its optical/UV/X-ray observations. Photoionisation models are presented in Section 4. The location of an absorber and connection to an accretion disk atmosphere is discussed in Sec. 5 and Sec. 6 respectively. We summarise our results in Sec. 7.

2. The source

Recently observed high redshift quasar HS 1603+3820 with $z_{\text{em}} = 2.54$ indicates extreme richness of absorption lines in its spectra (Dobrzycki et al., 1999; Misawa et al., 2003, 2005, Paper I).

The source was first discovered in the Hamburg/CfA Bright Quasar Survey (Hagen et al., 1995; Dobrzycki et al., 1996). With the brightness $B = 15.9$, it is among the top few brightest quasars known at such redshift. However, the most striking feature of HS 1603+3820 is its absorption spectrum, which indicates the presence of ~ 50 individual absorption systems, with 30+ of them having velocities higher than 10000 km s^{-1} , when corrected for quasar redshift based on emission lines. Many - perhaps all - of these clouds are physically associated with the quasar, particularly because some lines show variability in the timescales of a few years (Misawa et al., 2007).

High resolution observations from Subaru telescope with the High Dispersion Spectrograph, reported by Misawa et al. (2003, 2005) enabled to resolve many of those systems into a number of narrow components. The authors grouped the absorbers into several systems, designated with the letters from A to H.

All of those systems, and two previously unknown, were indicated in the observations taken by MMT and Keck telescope and reported in Paper I. Furthermore, the authors have noticed that some clouds in system A have a high ratio of C IV to H I column densities, reaching ~ 20 . System A, and other systems spatially close to the quasar can be used as a probe for the intrinsic emission of the quasar itself, since the conditions in the systems are undoubtedly heavily influenced by the quasar flux (e.g. Crenshaw et al., 2003; Gabel et al., 2005; Scott et al., 2005, and references therein).

Additionally, in Paper I, X-ray *Chandra* observations of HS 1603+3820 were reported, allowing to calculate the relative optical-to-X-ray slope, $\alpha_{\text{ox}} = 1.49$, which is typical for a quasar at this redshift (Bechtold et al., 2003).

3. Observational constrains important for photoionisation modelling

To explain the properties of an intrinsic absorption in HS 1603+3820 we need to construct illuminated continuum which affects absorbing gas. The observational data used in this paper are described in detail in Paper I. In subsections below, we shortly remind the reader values of fitted parameters for those observations, and summarise what is important for our modelling.

3.1. Continuum shape and normalisation

The optical/UV data spectrophotometry was taken from Scott et al. (2000), and it was obtained on July 4, 1995 with Stewart Observatory Bok Telescope. Our continuum fit results with power-law photon index $\Gamma_{UV} = 1.36 \pm 0.1$. Observed optical flux at $\lambda_{\text{rest}} = 1450 \text{ \AA}$ ($E_{\text{rest}} = 8.55 \times 10^{-3} \text{ keV}$) is $EF_E(B) = 3.20 \times 10^{-12} \text{ erg s}^{-1} \text{ cm}^{-2}$ as reported by Scott et al. (2000) (see their Tab. 3). In Fig. 1, blue points represent overall normalised flux in optical/UV domain.

The X-ray data were taken with the *Chandra X-ray Observatory* on 2002 November 29. We performed the fit assuming the intrinsic quasar spectrum to be a power law, with fixed Galactic absorption towards HS 1603+3820 of $N_{\text{H}} = 1.3 \times 10^{21} \text{ cm}^{-2}$. The best fit gave the photon index of $\Gamma_X = 1.91 \pm 0.20$ and normalisation at the rest frame for 1 keV of $A = (2.43 \pm 0.79) \times 10^{-4} \text{ photons cm}^{-2} \text{ s}^{-1} \text{ keV}^{-1}$. The X-ray part of observed and modelled spectrum is presented in the Fig. 1, red squares.

HS 1603+3820 has been pointed at with IUE/LWP on 1995-08-19, but not detected. The observation gave the upper limit of $1.5 \times 10^{-15} \text{ erg s}^{-1} \text{ cm}^{-2} \text{ \AA}^{-1}$ in the 2200-3100 \AA (observed) wavelength range. This limit is marked in green on Fig. 1. We note that this wavelength range covers the inferred position of Lyman-limit absorption from associated absorbers. It is therefore possible that this limit does not reflect low QSO's intrinsic luminosity in this range, although the individual absorbers do not appear to have sufficient column densities.

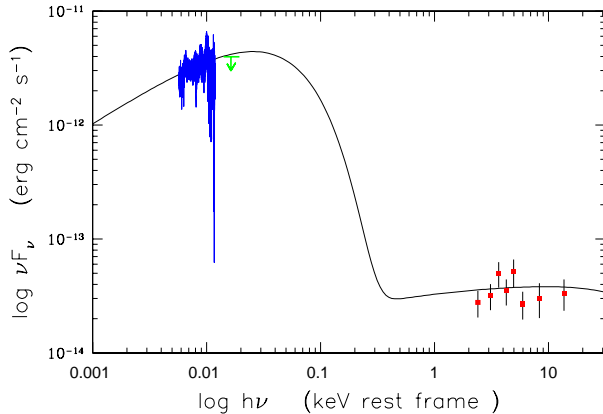


Figure 1: Normalised multi-band spectrum of HS 1603+3820 from MMT and Keck (blue points), IUE upper limit (green arrow), and Chandra (red squares) in the rest frame of quasar. Solid line represents the best shape of modelled spectrum used in calculations of photoionised intrinsic absorber presented in Sec 4.

Table 1: Ratios of ionic column densities of C_{iv} and H_i observed in intrinsic absorption system A1, obtained for various assumptions about the covering factor of H_i cloud and fitting methods for system A1 ($z_{abs} = 2.41941 \pm 0.00002$). The name of the system and the No. Line ID are taken after our Paper I.

Sys. No.	$\log(N_{Civ})$	$c_f(N_{Civ})$	$b(N_{Civ})$	$\log(Hi)$	$c_f(Hi)$	$b(Hi)$	N_{Civ}/N_{Hi}
A1 ^g	14.97 ± 0.04	0.36	72 ± 3	13.65 ± 0.03	0.61	62 ± 10	20.37 ± 2.70
A1	14.97 ± 0.04	0.36	72 ± 3	13.87 ± 0.05	1.00	145 ± 12	12.4 ± 2.10
A1	14.97 ± 0.04	0.36	72 ± 3	14.11 ± 0.05	0.61	132 ± 10	7.1 ± 1.20
A1	14.97 ± 0.04	0.36	72 ± 3	14.34 ± 0.05	0.36	75 ± 9	4.2 ± 0.70

^g global fit for all lines of system A from Paper I

We adopt those values for all photoionisation models in Sec. 4, and for an estimation of bolometric luminosity in Sec. 5. We present the overall continuum in Fig. 1. Note that different parts of the spectrum are taken at different epochs therefore SED constructed by us can contain systematic errors. Nevertheless, for the time being, there is no other way to find continuum for this quasar.

3.2. Optical/UV spectroscopy and parameters from spectral lines fitting

HS 1603+3820 has been observed with two instruments. On 2001 August 19 we used the Echelle Spectrograph and Imager (Sheinis et al., 2002) on the Keck II telescope, with the combined exposure of 4800 sec. The 0.5 arcsec slit was used, yielding the resolution of 45-50 km s⁻¹.

Full procedure of spectral line fitting of optical/UV HS 1603+3820 spectrum is presented in Paper I. The line profile fits were performed using VPGUESS/VPFIT programmes¹. We were able to fit simultaneously several lines from different ions, but characterised by the same redshift.

In several clouds belonging to an intrinsic absorption systems the column density of C_{iv} ion is bigger than the column density of ionised hydrogen H_i. The cloud A1 was an extreme example, with the ratio of N_{Civ}/N_{Hi} equal 20 ± 3 . In the present paper we concentrate on modelling this component in detail.

In Paper I, the covering factor for the hydrogen and for carbon fitting were found to be different (0.36 and 0.61, correspondingly) which could argue against a single well defined cloud responsible for A1 absorption. However, the kinematic width of the lines were similar. Therefore, we reconsidered the spectroscopic data by performing fits specifically for the component A1, instead of assuming the same covering factor for all clouds in component A. The old result and new results are given in Tab. 1.

¹<http://www.eso.org/~jliske/vpguess/>, <http://www.ast.cam.ac.uk/~rfc/vpfit.html>

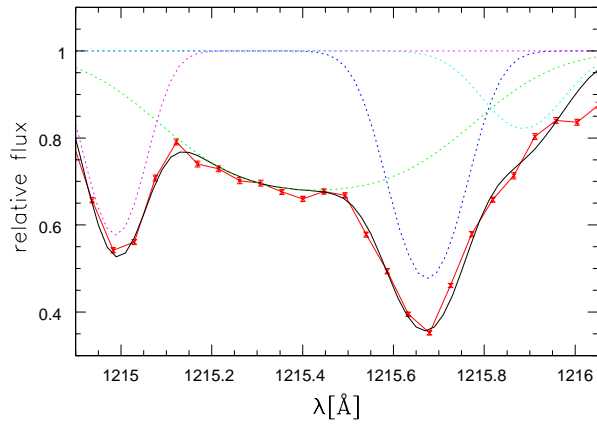


Figure 2: The fit of the Ly α region for A1 component taking covering factor equal 0.36, as for C1v . Broad green dotted line represents an H I line of intrinsic absorber, other magenta and blue components represent Ly α forest, red dots and line are observed Keck data, and black continuous line is the final model.

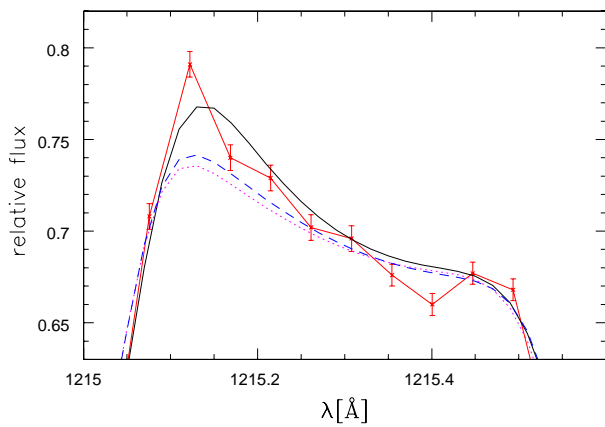


Figure 3: Enlarged part of Fig. 2 where the Ly α region of the A1 component is fitted with three different covering factors for H I absorber. Solid-black line is for covering factor equal 0.36, dashed-blue - 0.61, and dotted-red - 1, i.e. complete covering. Again data from Keck are marked by red points and line.

In Fig. 2 we show that the covering factor implied for CIV component can provide good fit to the H α component. Thus both covering factor and the kinematic width are the same for the two elements, and the absorption is likely coming from a single cloud. The fit is actually somewhat better for low covering factor although the results are not firm since we see well only a fraction of the line due to overlapping narrower components from Ly α forest (see Fig. 3).

Although the errors are huge, the values of ratio are always much higher than unity, which indicates either overabundance of carbon, or peculiar photoionisation model. For farther analyses we refer to the value of that ratio equal 20, as found in Paper 1.

4. Photoionisation models

In order to explain high ratio of N_{Civ} to the $N_{H\alpha}$ in the absorbing medium of the HS 1603+3820 we perform photoionisation calculations using two codes: CLOUDY (Ferland et al., 1998) version 08 and TITAN (Dumont et al., 2000).

We model the broad band spectrum of HS 1603+3820 shown in Fig. 1 using two power law components, both with an exponential cut-off at low and high energies:

$$F_E = E^{-\alpha} \exp(-E/E_{max}) \exp(-E_{min}/E), \quad (1)$$

where spectral index $\alpha = \Gamma - 1$, as usual. The first power law represents the optical/UV spectrum: $\alpha_{UV} = 0.36$, $E_{min}^{UV} = 1.36 \times 10^{-4}$ keV, with E_{max}^{UV} being first free parameter of the model, and the second power law represents the X-ray emission ($\alpha_X = 0.91$, $E_{min}^X = E_{max}^{UV}$, $E_{max}^X = 100$ keV).

The important parameter is UV power-law high energy cut-off, since it regulates amount of soft photons affecting the absorber. For the solid line in the Fig. 1, which represents the best shape of modelled spectrum, the value $E_{max}^{UV} = 40$ eV. But this value is not well constrained since we don't have enough far-UV observational points to determine overall curvature of the quasar spectrum, and since we do not consider any spectral variability. Alternatively, the transition between power-laws can be sharp with $E_{max}^{UV} = 10$ eV. Therefore, we adopt the value of E_{max}^{UV} as a free parameter of the model.

Other parameters needed for photoionisation calculations are set in a standard way. We use the ionisation parameter defined as:

$$\xi = \frac{L}{n_0 R^2}, \quad (2)$$

where L is the quasar bolometric luminosity, n_0 is the hydrogen number density at the cloud illuminated surface, and R is the distance of the intrinsic absorber from an UV/X-ray source, i.e. quasar nucleus. In all computations presented below, we calculate grid of models for different ξ , n_0 and R , fixing the total quasar bolometric luminosity at $L = 10^{46}$ erg s $^{-1}$. For photoionisation modelling it is no important what value of L we assume, since it can be modified by moving cloud closer or farther from the nucleus.

4.1. Modelling with CLOUDY

All photoionisation models computed by CLOUDY assume transmission of UV/X-ray flux through a constant density slab, which in such case is equal to surface hydrogen density number, n_0 . We have calculated large grid of models for different high energy cut-offs in UV band, E_{max}^{UV} , ranging from 3 eV up to 42 eV, and different ionisation parameters, ξ , from 10^{-2} up to 2.5×10^4 .

The calculations were repeated for several distances, R , from the quasar nucleus, equal: $\log(R) = 16, 16.7, 17, 18, \text{ and } 20$ [cm]. The choice of distances was made to cover all expected locations of the absorber, either close to the nucleus, at $R = 0.00324$ pc, or far away from the central black hole, at $R = 32.4$ pc. Since bolometric luminosity is the same for all models, the density of the slab is calculated from Eq. (2), and spans range from 10^2 up to 10^{14} cm $^{-3}$.

Since column densities of ions can vary rapidly approaching the hydrogen ionisation front, located typically at $\log(N_{\text{H}}^{\text{tot}}) \sim 20.6$ [cm $^{-2}$] (see Fig. 1 in Korista et al., 2008), we consider two cases of clouds. One optically thin, with total hydrogen column density equal to $\log(N_{\text{H}}^{\text{tot}}) = 19$ [cm $^{-2}$], and one optically thick, with column density $\log(N_{\text{H}}^{\text{tot}}) = 22$ [cm $^{-2}$].

In Fig. 4 we present the ratios of ionic column densities of Civ and H α for different ionisation parameters and UV high energy cut-offs, for clouds with total column density $\log(N_{\text{H}}^{\text{tot}}) = 19$ [cm $^{-2}$]. Uppermost panel shows results for

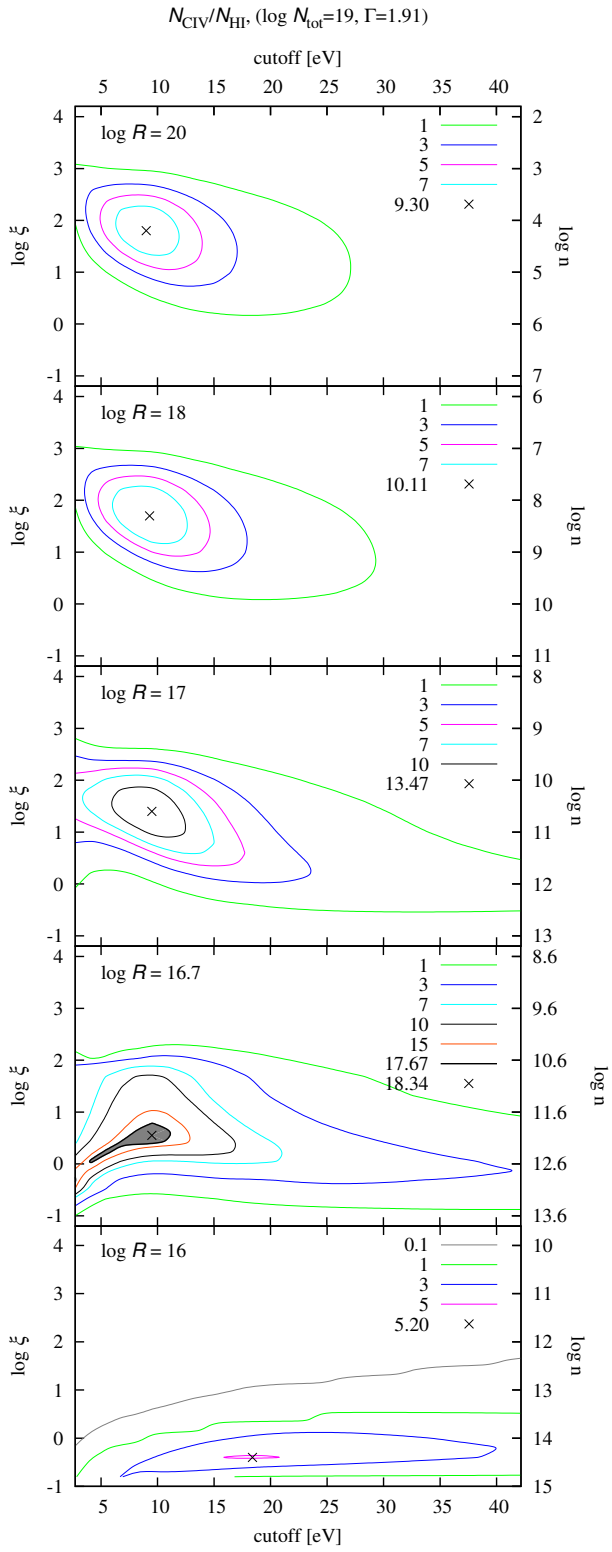


Figure 4: Contour plots for the ratio of CIV to HI column densities from cloudy for clouds with total column density $\log(N_{\text{H}}^{\text{tot}}) = 19$ [cm^{-2}].

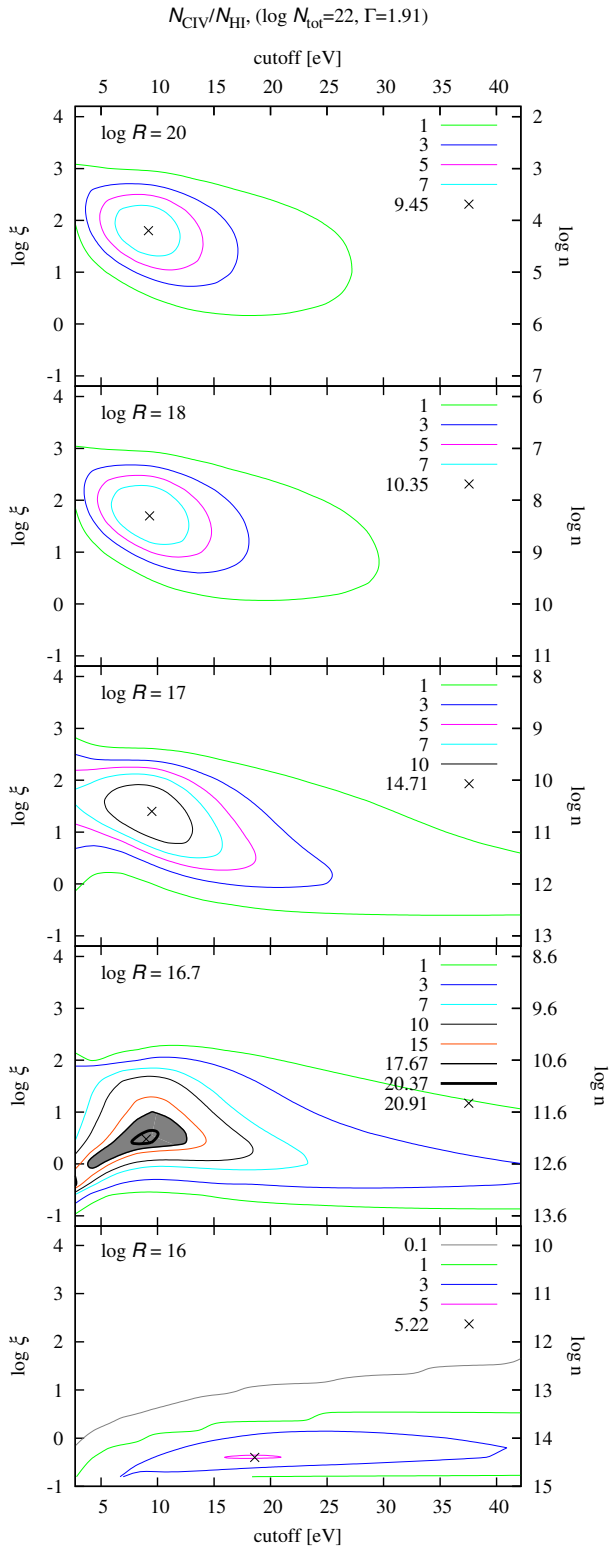


Figure 5: Contour plots for the ratio of CIV to HI column densities from cloudy for clouds with total column density $\log(N_{\text{H}}^{\text{tot}}) = 22$ [cm^{-2}].

absorber located farthest away from a nucleus at $\log(R) = 20$ [cm]. Lower panels represent absorbers closer to the quasar centre, and distances are marked in their upper-left corners. The value of ionisation parameter is shown on left vertical axis, the E_{max}^{UV} on the horizontal axis, while hydrogen density number, equal n_0 , on right vertical axis. Colour contours depict the values of ratio marked in upper-right corners of each panel.

Clouds located farther from the UV/X-ray source have low densities, and the ratio of N_{Civ} / N_{Hi} never exceeds 11. The highest value of N_{Civ} / N_{Hi} is achieved for absorber located at $\log(R) = 16.7$ [cm] and reaches 18.34.

The same grid of models but for $\log(N_H^{tot}) = 22$ [cm^{-2}] is presented in Fig. 5. Only for the dense cloud, $n_0 = 10^{12} \text{ cm}^{-3}$, located close to the nucleus, $\log(R) = 16.7$ [cm], the ratio of N_{Civ} / N_{Hi} reaches 20, which agrees with our observational result presented in Tab. 1, first row, so we accept this model for farther considerations in Sec. 5 below.

Finally, in Fig. 6, we present the set of clouds similar like in Fig. 4 computed with twice higher abundance of carbon. We see, that the distance for which the ratio of N_{Civ} / N_{Hi} is above 20 appeared for $\log(R) = 17$ [cm], so the distance increased by a factor of 2. For carbon abundance five times higher than solar in each distance there is a possibility to achieve an absorber with N_{Civ} / N_{Hi} above 20, and we are not able to find one photoionisation model which describes observations, therefore for further comparison we use only clouds with solar metallicity.

4.2. Modelling with TITAN

One of the key issues in understanding of the nature of the absorbing medium is its clumpiness. A clumpy medium can spontaneously form out of a continuous wind, if the condition for thermal instability is satisfied. An irradiated medium may indeed be a subject of thermal instability, as pointed out by Krolik et al. (1981), so a cold dense cloud can coexist with a hot rare medium under constant pressure and the size of the cloud is roughly determined by the Field length (Field, 1965; Begelman and McKee, 1990; Torricelli-Ciamponi and Courvoisier, 1998; Róžańska, 1999). It is therefore of interest to check whether the observed systems of clouds are consistent with the requirement of the thermal instability.

For that purpose, we consider the absorption by a cloud under constant pressure using the code TITAN, developed by Dumont et al. (2000). The code is designed to calculate the transmission of radiation through the cloud of considerable optical depth, since both the continuum and lines are calculated using the full radiative transfer instead of escape probability formalism. The density profile within the cloud is calculated self-consistently from the requirement of the total (i.e. radiation + gas) pressure being constant across the cloud (Róžańska et al., 2006). Since such numerical computations are time-consuming, we do not calculate an extended grid of models, but we aim to reproduce the observed C_{iv} to H_i ratio of HS 1603+3820.

We consider a range of the total column densities from 10^{21} up to 10^{23} cm^{-2} . Since we compute transfer through the cloud, we are able to make a plot of the ionisation parameter Ξ introduced by Krolik et al. (1981):

$$\Xi = \frac{F_{ion}}{cP_{gas}} = \frac{P_{rad}}{P_{gas}}, \quad (3)$$

which shows best the thermal instability region. For each of the model computed by TITAN we fix cut-off energy in UV/EUV band on the value $E_{max}^{UV} = 40$ eV. The free parameters of our model are the ionisation parameter ξ , and density number n_0 , both at the cloud surface, and the total column density N_H^{tot} . The method is illustrated in Fig. 7 where we show example of the temperature T vs. Ξ relation for several models. For the purpose of this paper we have calculated several clouds with following sets of parameters: cloud I: $n_0 = 10^{10} \text{ cm}^{-3}$, $\xi = 10^6$, $N_H^{tot} = 10^{23.3} \text{ cm}^{-2}$; cloud II: $n_0 = 10^{10} \text{ cm}^{-3}$, $\xi = 10^4$, $N_H^{tot} = 10^{22.7} \text{ cm}^{-2}$; cloud III: $n_0 = 10^8 \text{ cm}^{-3}$, $\xi = 10^6$, $N_H^{tot} = 10^{22} \text{ cm}^{-2}$; cloud IV: $n_0 = 10^9 \text{ cm}^{-3}$, $\xi = 10^4$, $N_H^{tot} = 10^{22} \text{ cm}^{-2}$; and cloud V: $n_0 = 10^{10} \text{ cm}^{-3}$, $\xi = 5 \times 10^3$, $N_H^{tot} = 10^{22} \text{ cm}^{-2}$.

Even for the soft spectrum, in case of HS 1603+382, the instability is still present, contrarily to the previous expectations (Krolik et al., 1981), but it appears at much lower optical depth since the Compton temperature of the incident radiation flux is considerably lower. Such a lower optical depth is in agreement with relatively low column densities of specific ions in comparison with those detected in a number of Seyfert 1 galaxies (Róžańska et al., 2006, and references therein).

In Fig. 8, we present total column density of the cloud versus column density of C_{iv} in the left hand panel, and the ratio of N_{Civ} / N_{Hi} in the right panel for several models. The column density of C_{iv} is the monotonic function of total column density, but ratio tends to have maximum. The best representation of the observed C_{iv} content was obtained for $n_0 = 10^{10}$, $\xi = 10^4$, and $N_H^{tot} = 2 \times 10^{22} \text{ cm}^{-2}$ - marked as a red point in Fig. 8. For this model we achieved $\log(N_{Civ}) = 14.71$ [cm^{-2}] and $N_{Civ} / N_{Hi} = 19.70$, which is very similar to the values observed in system A1.

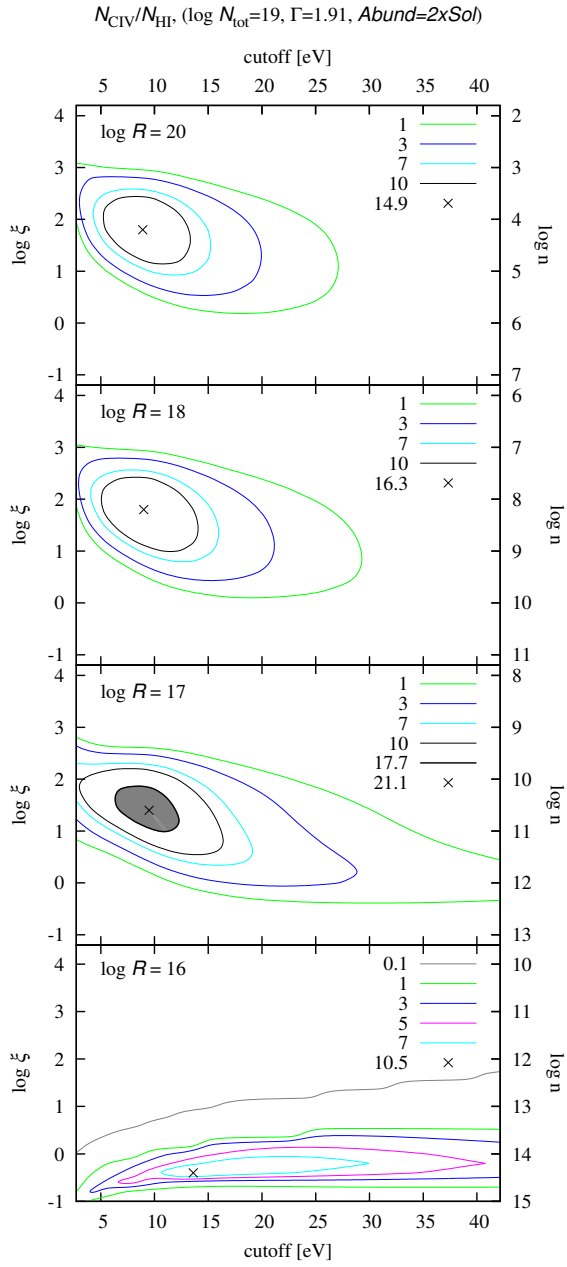


Figure 6: Contour plots for the ratio of CIV to HI column densities from CLOUDY for clouds with total column density $\log(N_{\text{H}}^{\text{tot}}) = 19$ [cm^{-2}], and with larger carbon abundance by a factor of 2.

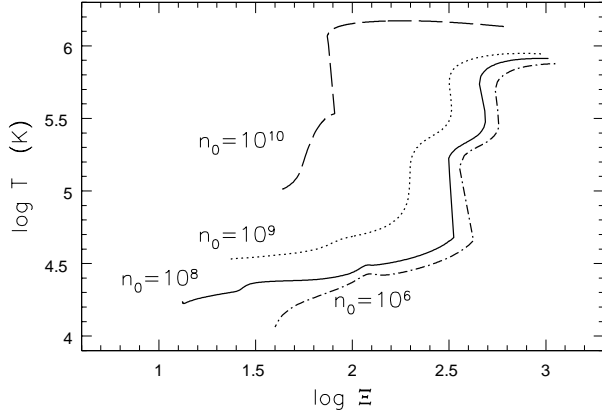


Figure 7: The stability curve, i.e. temperature versus ionisation parameter Ξ for constant pressure models computed by TITAN code. Different clouds are computed for the same ionisation parameter $\xi = 10^5$ (see Eq. (2)) at the cloud surface, and the same total column density $N_{\text{H}}^{\text{tot}} = 10^{22} \text{ cm}^{-2}$. Different hydrogen number densities on the cloud surfaces are presented by: long-dashed line - $n_0 = 10^{10}$, dotted line - $n_0 = 10^9$, solid line - $n_0 = 10^8$, and dashed-dotted line - $n_0 = 10^6 \text{ cm}^{-3}$.

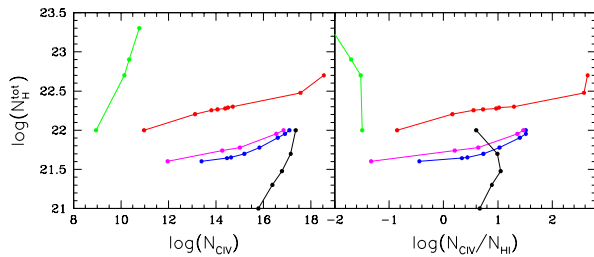


Figure 8: Total column density versus column density of Civ - left panel, ratio of $N_{\text{Civ}}/N_{\text{Hi}}$ - right panel, for different constant pressure clouds. Green solid line represents models for $n_0 = 10^{10} \text{ cm}^{-3}$ and $\xi = 10^6$, red line represents models for $n_0 = 10^{10} \text{ cm}^{-3}$ and $\xi = 10^4$, magenta line for $n_0 = 10^8 \text{ cm}^{-3}$ and $\xi = 10^6$, blue line for $n_0 = 10^9 \text{ cm}^{-3}$ and $\xi = 10^4$, and black line for $n_0 = 10^{10} \text{ cm}^{-3}$ and $\xi = 5 \times 10^3$. Each computed cloud is represented by point on those panels.

Note, that for constant pressure clouds, there are models presented by magenta and blue points with, $n_0 = 10^8$ and 10^9 cm^{-3} respectively, with ratio of $N_{\text{Civ}}/N_{\text{Hi}}$ approaching 20, but at the same time column density of Civ is huge i.e. $\log(N_{\text{Civ}}) = 16 - 17 [\text{cm}^{-2}]$ for those models, and exceeds the value appropriate for the A1.

5. Distance to the A1 absorber

In the aim to estimate the distance to the A1, we have to know bolometric luminosity of the quasar. Then, the photoionisation modelling presented above together with the observational constrains allows us to conclude that the best representation of system A1 is cloud with $\xi = 7$ and $n_0 = 10^{12}$ from CLOUDY and with $\xi = 10^4$ and $n_0 = 10^{10}$ from TITAN. The huge difference in ionisation parameter on the cloud surface is because a cloud computed by TITAN is stratified and contains both hot and cold phases (see Fig. 7), and a cloud computed by CLOUDY contains only cold phase of the absorber. Finally, after manipulating of equation (2) we derive the distance.

The most important is thus to estimate bolometric luminosity of the considered quasar. Misawa et al. (2005) gave the value of bolometric luminosity based on the prescription of Narayanan et al. (2004), where:

$$L_{\text{bol}} \approx 4.4 \lambda L_{\lambda} \quad \text{at} \quad \lambda = 1450 \text{ \AA}. \quad (4)$$

For HS 1603+3820 Misawa et al. (2005) have obtained $L_{\text{bol}} = 2.5 \times 10^{48} \text{ ergs s}^{-1}$. We did similar evaluation, besides that we have adopted the value of $f_{\nu}^{\text{obs}} = 550 \mu\text{Jy}$ at $\lambda = 1450 \text{ \AA}$, as reported for this quasar by Scott et al. (2000) (see their Tab. 3). Assuming standard cosmological parameters: $H_0 = 72 \text{ km s}^{-1} \text{ Mpc}^{-1}$, $\Omega_M = 0.3$, and

Table 2: Distance derivations based on CLOUDY and TITAN modelling for the A1 in HS 1603+3820, for solar metallicity. Middle rows contain results based on bolometric luminosity calculated in this paper from Eq. (4) using flux reported by Scott et al. (2000). Bottom rows - the one calculated by Misawa et al. (2005). Ionisation parameter, ξ on the surface of the cloud drops significantly inside the cloud for the TITAN model, and remains constant for CLOUDY model. See text for explanation.

Par.	Unit	CLOUDY	TITAN
ξ	[erg s ⁻¹ cm ⁻¹]	7	10 ⁴
n_0	[cm ⁻³]	10 ¹²	10 ¹⁰
E_{max}^{UV}	[eV]	10	40
$\log(N_{Civ})$	[cm ⁻²]	14.97	14.71
N_{Civ}/N_{Hi}		20.37	19.70
$L_{bol} = 7.7$	$\times 10^{47}$ [erg s ⁻¹]	This paper	
$\log(R)$	[cm]	17.52	16.94
R	[pc]	0.106	0.028
$L_{bol} = 2.5$	$\times 10^{48}$ [erg s ⁻¹]	Misawa 05	
$\log(R)$	[cm]	17.78	17.20
R	[pc]	0.192	0.051

$\Omega_\Lambda = 0.7$ for luminosity distance, and using Eq. (4), we have computed that $L_{bol} = 7.7 \times 10^{47}$ erg s⁻¹. This value is lower from that obtained by Misawa et al. (2005), by a factor of 3.25. Note, that such derivation of bolometric luminosity has the factor of two uncertainty.

Taking into account both values of bolometric luminosities, we derive the distance to the A1 for models computed by CLOUDY and TITAN.

Regardless of the value of L_{bol} , in each case the A1 absorber is located very close to the quasar nucleus within $R = 0.1 - 0.2$ pc. Our results differ from these obtained by Misawa et al. (2005, 2007) using variability method Hamann et al. (1997). Assuming that variability is caused by the change of ionisation, they found for $\Delta t \sim 0.36$ yr the location of system A within $r < 6$ kpc, and for 1.2 yr the location of the mini-BAL in system A within $r < 8$ kpc (Misawa et al., 2005).

Nevertheless, our results are in agreement with dynamical model of Murray and Chiang (1995) adopted for HS 1603+3820 by Misawa et al. (2005) (see Sec. 6.2). Using the relation for the radius of the gas parcel relative to its launch radius, they have obtained constraint of $r < 0.2$ pc for system A. All distance derivations are given in Table 2.

Our results are less restrictive if the lower value of the C_{iv} to H_i ratio is used, or metallicity is allowed to be higher. The increase in the metallicity by a factor of two moves the upper limit for the distance also by a factor of 2. However, if we adopt lower cloud covering factor and, in consequence lower value of the N_{Civ}/N_{Hi} ratio, the upper limit for the cloud distance moves to the 30 pc. The lower limit to the distance remains practically unchanged.

6. Connection with an accretion disk and BLR

The distance to the A1 absorber of HS 1603+3820 derived by us suggests that the absorbing material may be connected with the wind from an accretion disk atmosphere. Upper atmospheric layers can be quite dense up to $n_H \sim 10^{14}$ cm⁻³, depending on the distance from the central black hole as pointed by Hryniewicz (2011). Such density can be calculated by solving an accretion disk vertical structure parametrised by the black hole mass, its spin and the accretion rate (Róžańska et al., 1999). We can properly derive density at $\tau \sim 2/3$, since we assume diffusion approximation for radiation when solving the disk vertical structure. This approximation is valid for the disk interior, but does not solve properly the structure of outer atmosphere at $\tau \ll 1$. However, the density at $\tau = 2/3$ is representative as an initial density in the disk wind, which supplies matter to the BLR or other intrinsic absorber.

Radial profile of the density atmosphere at the optical depth $\tau \sim 2/3$, in an accretion disk around non-rotating black hole in the centre of weak line quasar SDSS J0945533.99+100950 is presented in Hryniewicz (2011). Authors have shown visible bump in disk's density distribution caused by the drop of the opacity in the region where the

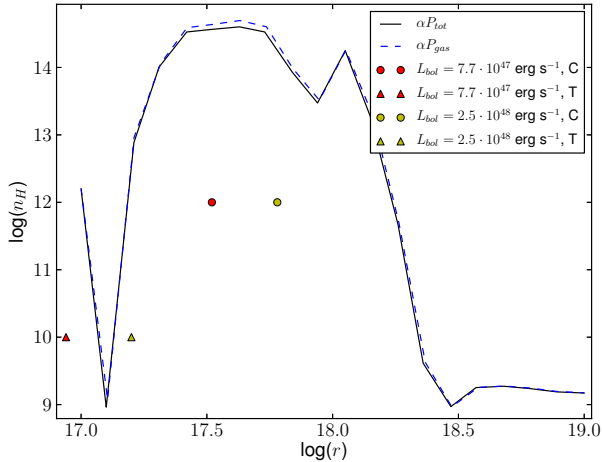


Figure 9: The value of number density on the disk surface, calculated from an accretion disk vertical structure (see Sec. 5 for explanation), versus the distance from the quasar centre. Two radial profiles (blue and black) are calculated for two viscous heating prescription marked in the left upper corner. Points represent values achieved for both parameters from photoionisation modelling. Clouds computed with CLOUDY (C), are marked by circles, and those computed with TITAN (T) - by triangles. Red points represent clouds with bolometric luminosity calculated by us, while green points - by Misawa et al. (2005).

temperature is too low for significant contribution of electron scattering and free-free processes (Hure et al., 1994) but still too high for opacity due to the dust, so only molecules are the source of opacity. Sudden drop of the volume hydrogen density from 10^{14} to 10^9 cm^{-3} occurs at $\log(R) \sim 18$ [cm] (see Fig. 5 in Hryniewicz (2011)), and coincides perfectly with the distance to BLR for this object.

We have made the same calculations for the mass of the black hole appropriate for HS 1603+3820, derived from bolometric luminosity $L_{bol} = 7.7 \times 10^{47}$ erg s^{-1} , assuming mass accretion rate equal Eddington, black hole mass is $M_{BH} = 5.26 \times 10^9 M_{\odot}$. Furthermore, we have estimated black hole mass in this quasar using CIV line (Vestergaard and Peterson, 2006), which gives similar value $M_{BH} = 5.4 \times 10^9 M_{\odot}$, with uncertainty of one order of magnitude.

Taking into account bolometric luminosity derived by us, we consider an accretion disk around black hole of the mass $5.26 \times 10^9 M_{\odot}$, and we assume Eddington accretion rate for the gas. For such disk we have computed radial profile of the density n_H at $\tau = 2/3$, assuming two different viscous heating prescriptions. First, we assume that viscous heating is proportional only to the gas pressure, so we do not expect any radiation pressure instabilities. Second, we assume that viscous stress is proportional to the total pressure.

Fig. 9 presents radial profiles of n_H , for two different viscosity prescriptions. The drop in the density of the disk atmosphere at the radius $\log(R) \sim 17$ [cm] is related to the partial ionisation of the hydrogen in the disk atmosphere and a very strong inversion in the vertical density profile due to radiation pressure. This partial ionisation effect is not related to the overall disk instability since the ionisation instability operates when there is partial ionisation of the disk interior (i.e. further out). What is more, if we change the viscosity prescription from αP_{tot} to αP_{gas} , the plot practically does not change, although the integrated disk surface density, Σ , changes more than by an order of magnitude. Such a strong density inversion in the disk atmosphere can lead to local instabilities and an outflow. Additionally, all points from our modelling are marked on this diagram. They are in good agreement with values predicted for outer layers of an accretion disk atmosphere around black hole with mass estimated by us from observational constrains.

Furthermore, following equation (3) in Pian et al. (2005), we can calculate the distance to the BLR in HS 1603+3820, from the continuum luminosity at 1350 \AA . Estimation is rather crude, since absorption can be present at this wavelength, but we have got the value of $\log(R_{BLR}) = 18.75$ [cm]. Together with our distance derivation to the A1 absorber, we conclude that intrinsic absorption is located in radial direction closer to the nucleus than a possible BLR in HS 1603+3820.

7. Conclusions

We have presented photoionisation modelling of intrinsic absorber in quasar HS 1603+3820. Using observations from optical/UV/X-ray energy bands, we have constructed the shape of continuum, which interacts with absorbers on the way from the nucleus. Double power-law with exponential cut-offs and related observed optical to X-ray slope $\alpha_{ox} = 1.49$, was adopted as an input to photoionisation modelling of the first cloud in system A.

For several lines of system A1, reported in Paper I, we have found very high ratio of column densities of C IV to H I. The value of this ratio in some cases exceeds 20. Our photoionisation computations done by CLOUDY and TITAN show that this value, together with intrinsic SED of HS 1603+3820, allowed us to choose a single solution which explains all observational constrains.

From modelling done by TITAN, we found that total column density of absorbing system is $2 \times 10^{22} \text{ cm}^{-2}$. This value is quite close to the maximum column density in a constant pressure medium due to the thermal instability. It is one order of magnitude lower than the values derived for Seyfert galaxies (Róžańska et al., 2008), since the intrinsic spectrum of HS 1603+3820 is much softer, with a very weak X-ray tail. This coincidence supports the view that intrinsic absorbers do form in the wind as a result of thermal instability and the constant pressure model is better suited to interpret the data than the constant density one.

The hydrogen number density derived from modelling is rather high, of the order of $n = 10^{10}, 10^{12} \text{ cm}^{-3}$, which is consistent with previous density estimations of UV intrinsic absorbers in NLS1 galaxies (see Leighly (2004)). On the other hand, our result is inconsistent with number density found by Misawa et al. (2005) using variability method.

Such high value of number density gives the location of absorbing gas quite close to the nucleus within $R = 0.1 - 0.2 \text{ pc}$. This location supports scenario that UV/X-ray outflows are in the form of winds from accretion disk atmospheres with similar number densities. Furthermore, we have shown that the A1 absorber is located closer to the nucleus than the BLR for a given bolometric luminosity of HS 1603+3820.

The results, however, are very sensitive to the measured C IV to H I ratio, which is sensitive to the determination of the covering factor, very difficult for hydrogen line. For the same covering factor for H I and C IV of 0.36 in the Keck 2001 data, the ratio is much lower than measured in Paper I and the upper limit for the distance is moves to 30 pc. Also assumption of higher metallicity increases the upper limit for the absorber distance.

Close location of the absorber system is in contradiction with Misawa et al. (2005, 2007) who found that system A is located within $r = 6 \text{ kpc}$, but it agrees with dynamical model of (Murray and Chiang, 1995) adopted for HS 1603+3820 by (Misawa et al., 2005) (see Sec. 6.2). Using the relation for the radius of the gas parcel relative to its launch radius, they have obtained constraint of $r < 0.2 \text{ pc}$ for system A.

The outflow velocities of system A are rather high, up to few thousands km s^{-1} , which is consistent with the winds detected in X-rays in several NLS1. Therefore, HS 1603+3820 can be considered as a high redshift analog of NLS1 galaxies.

Acknowledgements

We thank A. Gawryszczak for his help with model computations. Support for this work was provided by grant 2011/03/B/ST9/03281, 2012/04/M/ST9/00780, and NN203 581240 the Polish National Science Center. Some of the data presented in this paper were obtained from the Multimission Archive at the Space Telescope Science Institute (MAST). STScI is operated by the Association of Universities for Research in Astronomy, Inc., under NASA contract NAS5-26555. Support for MAST for non-HST data is provided by the NASA Office of Space Science via grant NAG5-7584 and by other grants and contracts.

References

- Arav, N., Brotherton, M. S., Becker, R. H., Gregg, M. D., White, R. L., Price, T., Hack, W., Jan. 2001. The Intrinsic Absorber in QSO 2359-1241: Keck and HUBBLE SPACE TELESCOPE Observations. *ApJ* 546, 140–149.
- Bautista, M. A., Dunn, J. P., Arav, N., Korista, K. T., Moe, M., Benn, C., Apr. 2010. Distance to Multiple Kinematic Components of Quasar Outflows: Very Large Telescope Observations of QSO 2359-1241 and SDSS J0318-0600. *ApJ* 713, 25–31.
- Bechtold, J., Siemiginowska, A., Shields, J., Czerny, B., Janiuk, A., Hamann, F., Aldcroft, T. L., Elvis, M., Dobrzycki, A., May 2003. Chandra Survey of Radio-quiet, High-Redshift Quasars. *ApJ* 588, 119–127.
- Begelman, M. C., McKee, C. F., Aug. 1990. Global effects of thermal conduction on two-phase media. *ApJ* 358, 375–391.

- Blustin, A. J., Page, M. J., Fuerst, S. V., Branduardi-Raymont, G., Ashton, C. E., Feb. 2005. The nature and origin of Seyfert warm absorbers. *A&A* 431, 111–125.
- Chakravorty, S., Kembhavi, A. K., Elvis, M., Ferland, G., Feb. 2009. Properties of warm absorbers in active galaxies: a systematic stability curve analysis. *MNRAS* 393, 83–98.
- Crenshaw, D. M., Kraemer, S. B., Boggess, A., Maran, S. P., Mushotzky, R. F., Wu, C., May 1999. Intrinsic Absorption Lines in Seyfert 1 Galaxies. I. Ultraviolet Spectra from the Hubble Space Telescope. *ApJ* 516, 750–768.
- Crenshaw, D. M., Kraemer, S. B., Gabel, J. R., Kaastra, J. S., Steenbrugge, K. C., Brinkman, A. C., Dunn, J. P., George, I. M., Liedahl, D. A., Paerels, F. B. S., Turner, T. J., Yaqoob, T., Sep. 2003. Simultaneous Ultraviolet and X-Ray Spectroscopy of the Seyfert 1 Galaxy NGC 5548. I. Physical Conditions in the Ultraviolet Absorbers. *ApJ* 594, 116–127.
- Dobrzycki, A., Engels, D., Hagen, H.-J., Sep. 1999. HS 1603+3820: a bright $z_{\text{em}}=2.51$ quasar with a very rich heavy element absorption spectrum. *A&A* 349, L29–L33.
- Dobrzycki, A., Engels, D., Hagen, H.-J., Elvis, M., Huchra, J., Reimers, D., May 1996. The Hamburg-CfA Quasar Survey. *BAAS* 28, 829–+.
- Dobrzycki, A., Nikolajuk, M., Bechtold, J., Ebeling, H., Czerny, B., Rózańska, A., Dec. 2007. Absorption spectrum of the quasar HS1603+3820. I. Observations and data analysis. *A&A* 476, 1205–1217.
- Dumont, A.-M., Abrassart, A., Collin, S., May 2000. A code for optically thick and hot photoionized media. *A&A* 357, 823–838.
- Ferland, G. J., Korista, K. T., Verner, D. A., Ferguson, J. W., Kingdon, J. B., Verner, E. M., Jul. 1998. CLOUDY 90: Numerical Simulation of Plasmas and Their Spectra. *PASP* 110, 761–778.
- Field, G. B., Aug. 1965. Thermal Instability. *ApJ* 142, 531–+.
- Gabel, J. R., Crenshaw, D. M., Kraemer, S. B., Brandt, W. N., George, I. M., Hamann, F. W., Kaiser, M. E., Kaspi, S., Kriss, G. A., Mathur, S., Mushotzky, R. F., Nandra, K., Netzer, H., Peterson, B. M., Shields, J. C., Turner, T. J., Zheng, W., Jan. 2003. The Ionized Gas and Nuclear Environment in NGC 3783. II. Averaged Hubble Space Telescope/STIS and Far Ultraviolet Spectroscopic Explorer Spectra. *ApJ* 583, 178–191.
- Gabel, J. R., Kraemer, S. B., Crenshaw, D. M., George, I. M., Brandt, W. N., Hamann, F. W., Kaiser, M. E., Kaspi, S., Kriss, G. A., Mathur, S., Nandra, K., Netzer, H., Peterson, B. M., Shields, J. C., Turner, T. J., Zheng, W., Oct. 2005. The Ionized Gas and Nuclear Environment in NGC 3783. V. Variability and Modeling of the Intrinsic Ultraviolet Absorption. *ApJ* 631, 741–761.
- Hagen, H.-J., Groot, D., Engels, D., Reimers, D., May 1995. The Hamburg Quasar Survey. I. Schmidt observations and plate digitization. *A&AS* 111, 195–+.
- Hamann, F., Barlow, T. A., Junkkarinen, V., Burbidge, E. M., Mar. 1997. High-Resolution Spectra of Intrinsic Absorption Lines in the Quasi-stellar Object UM 675. *ApJ* 478, 80.
- Hryniewicz, K., 2011. Is the SDSS J094533.99+100950.1 higher mass equivalent to narrow-line Seyfert 1 galaxies? In: *Narrow-Line Seyfert 1 Galaxies and their Place in the Universe*.
- Hure, J.-M., Collin-Souffrin, S., Le Bourlot, J., Pineau des Forets, G., Oct. 1994. Structure of the outer regions of accretion discs in Active Galactic Nuclei: the influence of opacity. *A&A* 290, 34–39.
- Kaastra, J. S., Steenbrugge, K. C., Raassen, A. J. J., van der Meer, R. L. J., Brinkman, A. C., Liedahl, D. A., Behar, E., de Rosa, A., May 2002. X-ray spectroscopy of NGC 5548. *A&A* 386, 427–445.
- Kaspi, S., Brandt, W. N., Netzer, H., George, I. M., Chartas, G., Behar, E., Sambruna, R. M., Garmire, G. P., Nousek, J. A., Jun. 2001. High-Resolution X-Ray Spectroscopy and Modeling of the Absorbing and Emitting Outflow in NGC 3783. *ApJ* 554, 216–232.
- Korista, K. T., Bautista, M. A., Arav, N., Moe, M., Costantini, E., Benn, C., Nov. 2008. Physical Conditions in Quasar Outflows: Very Large Telescope Observations of QSO 2359-1241. *ApJ* 688, 108–115.
- Krolik, J. H., Kriss, G. A., Jul. 1995. Observable Properties of X-Ray–heated Winds in Active Galactic Nuclei: Warm Reflectors and Warm Absorbers. *ApJ* 447, 512–+.
- Krolik, J. H., McKee, C. F., Tarter, C. B., Oct. 1981. Two-phase models of quasar emission line regions. *ApJ* 249, 422–442.
- Krongold, Y., Nicastro, F., Brickhouse, N. S., Elvis, M., Mathur, S., Apr. 2005. Opacity Variations in the Ionized Absorption in NGC 3783: A Compact Absorber. *ApJ* 622, 842–846.
- Leighly, K. M., Aug. 2004. Hubble Space Telescope STIS Ultraviolet Spectral Evidence of Outflow in Extreme Narrow-Line Seyfert 1 Galaxies. II. Modeling and Interpretation. *ApJ* 611, 125–152.
- Mathews, W. G., Ferland, G. J., Dec. 1987. What heats the hot phase in active nuclei? *ApJ* 323, 456–467.
- Misawa, T., Eracleous, M., Charlton, J. C., Kashikawa, N., May 2007. Results of Monitoring the Dramatically Variable C IV Mini-Broad Absorption Line System in the Quasar HS 1603+3820. *ApJ* 660, 152–166.
- Misawa, T., Eracleous, M., Charlton, J. C., Tajitsu, A., Aug. 2005. Time-Variable Complex Metal Absorption Lines in the Quasar HS 1603+3820. *ApJ* 629, 115–130.
- Misawa, T., Yamada, T., Takada-Hidai, M., Wang, Y., Kashikawa, N., Iye, M., Tanaka, I., Mar. 2003. Subaru High-Resolution Spectroscopy of Complex Metal Absorption Lines of the Quasar HS 1603+3820. *AJ* 125, 1336–1344.
- Moe, M., Arav, N., Bautista, M. A., Korista, K. T., Nov. 2009. Quasar Outflow Contribution to AGN Feedback: Observations of QSO SDSS J0838+2955. *ApJ* 706, 525–534.
- Murray, N., Chiang, J., Dec. 1995. Active Galactic Nuclei Disk Winds, Absorption Lines, and Warm Absorbers. *ApJL* 454, L105.
- Narayanan, D., Hamann, F., Barlow, T., Burbidge, E. M., Cohen, R. D., Junkkarinen, V., Lyons, R., Feb. 2004. Variability Tests for Intrinsic Absorption Lines in Quasar Spectra. *ApJ* 601, 715–722.
- Netzer, H., Kaspi, S., Behar, E., Brandt, W. N., Chelouche, D., George, I. M., Crenshaw, D. M., Gabel, J. R., Hamann, F. W., Kraemer, S. B., Kriss, G. A., Nandra, K., Peterson, B. M., Shields, J. C., Turner, T. J., Dec. 2003. The Ionized Gas and Nuclear Environment in NGC 3783. IV. Variability and Modeling of the 900 Kilosecond Chandra Spectrum. *ApJ* 599, 933–948.
- Nicastro, F., Fiore, F., Perola, G. C., Elvis, M., Feb. 1999. Ionized Absorbers in Active Galactic Nuclei: The Role of Collisional Ionization and Time-evolving Photoionization. *ApJ* 512, 184–196.
- Pian, E., Falomo, R., Treves, A., Aug. 2005. Hubble Space Telescope ultraviolet spectroscopy of blazars: emission-line properties and black hole masses. *MNRAS* 361, 919–926.
- Rózańska, A., Sep. 1999. Thermal conduction between an accretion disc and a corona in active galactic nuclei: vertical structure of the transition

- layer. MNRAS 308, 751–762.
- Róžańska, A., Czerny, B., Życki, P. T., Pojmański, G., May 1999. Vertical structure of accretion discs with hot coronae in active galactic nuclei. MNRAS 305, 481–491.
- Róžańska, A., Goosmann, R., Dumont, A.-M., Czerny, B., Jun. 2006. Modeling the warm absorber in active galactic nuclei. A&A 452, 1–13.
- Róžańska, A., Kowalska, I., Gonçalves, A. C., Sep. 2008. How to estimate the distance to the warm absorber in AGN from photoionized models. A&A 487, 895–900.
- Scott, J., Bechtold, J., Dobrzycki, A., Kulkarni, V. P., Sep. 2000. A Uniform Analysis of the Ly α Forest at $z=0-5$. II. Measuring the Mean Intensity of the Extragalactic Ionizing Background Using the Proximity Effect. ApJS 130, 67–89.
- Scott, J. E., Kriss, G. A., Lee, J. C., Quijano, J. K., Brotherton, M., Canizares, C. R., Green, R. F., Hutchings, J., Kaiser, M. E., Marshall, H., Oegerle, W., Ogle, P., Zheng, W., Nov. 2005. Intrinsic Absorption in the Spectrum of NGC 7469: Simultaneous Chandra, FUSE, and STIS Observations. ApJ 634, 193–209.
- Sheinis, A. I., Bolte, M., Epps, H. W., Kibrick, R. I., Miller, J. S., Radovan, M. V., Bigelow, B. C., Sutin, B. M., Aug. 2002. ESI, a New Keck Observatory Echellette Spectrograph and Imager. PASP 114, 851–865.
- Torricelli-Ciamponi, G., Courvoisier, T. J.-L., Jul. 1998. Optically thin thermal emission from cold clouds in active galactic nuclei. A&A 335, 881–893.
- Vestergaard, M., Peterson, B. M., Apr. 2006. Determining Central Black Hole Masses in Distant Active Galaxies and Quasars. II. Improved Optical and UV Scaling Relationships. ApJ 641, 689–709.
- Weymann, R. J., 1995. Broad Absorption Line Quasars: An Overview. In: G. Meylan (Ed.), QSO Absorption Lines. pp. 213–+.